International Conference on Mechanical and Industrial Engineering
ICMIE2022
November 15-17, 2022 Tripoli-Libya

The Assessment of the Simple Coupled Volume of Fluid and Level Set Algorithm in OpenFoam For Liquid Jet Atomization

Abdallah Salem

Department of Mechanical and Industrial Engineering University of Wadi- Alshatti, Libya
A.Salem@wau.edu.ly

Abstract—Improvements to the performance efficiency of the open source c++ library of incompressible two-phase flows solver in OpenFoam-v1706 software, namely interFoam in surface tension-dominated flows, are implemented. The new solver, SCLSVOF, is based on simple coupling between the Volume of Fluid and level set methods. We validated the new solver against interFoam on different tests, such as 2D droplet in vortical field, evaluating the pressure jump error across a static droplet for three different density ratios, and the decay rate of the standing capillary wave driven by surface tension force damped by viscosity. The test results obtained by the SCLSVOF method have shown that the advection error of the new algorithm is in the same order of magnitude as other approaches that use geometrical and algebraic techniques for the interface advection. Furthermore, an enhancement in the computation of the pressure jump across the static drop interface was achieved resulting in an error reduction of almost 8%. Additionally, the decay rate of the capillary wave computed by the SCLSVOF method is in better agreement with the analytical solution than those obtained by the interFoam method. Finally, the new solver was used to simulate a high-pressurized liquid jet in quiescent gas. The motion of the liquid jet and the formation of ligaments and droplets of different scales and smooth surfaces were well captured. The preliminary results showed that the incorporated SCLSVOF algorithm has promising potential in physically elucidating the atomization of the liquid jet.

Keywords— Volume of Fluid, Level Set, Turbulent Jet, interFoam, Atomization

I. INTRODUCTION

Atomization phenomenon is an important process in numerous engineering applications, such as aerospace propulsion systems, automotive engines, desalination plants, and spray coating systems [1]. Thus, a firm understanding of the atomization mechanisms in these applications can lead to better predictions of spray features, such as droplet size distribution and jet structure. Experimentally, observing the atomization mechanism in turbulent incompressible two-phase flows has been difficult. Many attempts reported experimental efforts to understand this phenomenon [1]. However, the resolution limit was bigger than the size of the primary breakup of the droplet. Therefore, attention has been shifted to numerical simulation to investigate the physics of the atomization process in any application, especially the breakup of fuel liquid in automotive and aerospace engines. One of the early attempts in the context of primary breakup simulations was the study of a liquid jet emanating into a quiescent gas carried out by Menard et al. [2]. The simulation was not considered a direct numerical simulation (DNS) for the given conditions as reported by Herrmann [1], yet the flow motion of the jet was captured. Another simulation in the same context was conducted by Desjardins et al. [3], where the level set and ghost fluid methods were implemented to capture the interface and handle the surface tension force, respectively. The phenomenon was well resolved for the prescribed flow conditions. One of the well-known and most advanced studies in this field is the one conducted by Shinjo et al. [4]. In their study, they used the coupled level set and volume of fluid method to implement a direct numerical simulation of fuel injected in quiescent pressurized gas using six billion grid points. They pointed out that once the jet emanates, it takes a mushroom like-shape. The first breakup process occurs at the edge of the mushroom jet tip due to strong gaseous shear force. The region behind the tip is highly disturbed, leading to more ligaments and droplet formation. Their simulation managed to elucidate unexpected atomization phenomena such as the creation of crests on the liquid surface, droplet re-collision with liquid jet, and the generation of droplets and ligaments from the liquid surface. However, conducting a numerical simulation of the turbulent liquid jet is not simple and requires two main tasks [1]. These are: tracking the interface between the liquid and the gas phases and accurate computation of the surface tension force responsible for the creation of droplets and ligaments. Moreover, the computational resources for these types of simulations are extremely expensive [4]. For capturing the phase interface, the Volume of Fluid (VOF) method first introduced by Hire et al. [5] identifies the volume fraction of each phase in the computational cell. This method has gained the advantage of being a robust mass-conserving technique [6]. However, the volume fraction distribution is discontinuous across the interface. Thus, poor prediction of the interfacial feature, such as the normal curvature, is obtaine. Another way to represent the interface is by using level set (LS) function first introduced by Dervieux et al. [7].

The level set is a sign distance function of a negative value at one phase, a positive value at the other phase, and a zero value at the interface. The Ls equation can be easily advected and solved. Therefore, it has the advantage of

better approximates interface features [2]. Yet, for flow fields with severe distortion, the function losses its property as a distance function, and a re-distancing process is required. To overcome the drawback of each method, LS and VOF are coupled to ensure both mass conservation by VOF and better approximation of interfacial local curvature computation by LS [8].

Many commercial and free software programs have recently been extensively used to simulate incompressible two-phase flows. One of those is interFoam, which has become highly attractive because it forms part of a suite of free, open-source C++ libraries of OpenFoam. Unlike most of the aforementioned studies where geometrical reconstruction of the interface is used to update the volume fraction flux, interFoam uses an algebraic algorithm based on the re-formulation of the pure Volume of Fluid advection equation. This approach proves its accuracy in capturing the interface and reduces the computational cost resulting from the interface reconstruction, especially in 3D problems. However, it has been shown that interFoam is less accurate when the role of surface tension becomes significant [9]. In the present study, the algorithm of simple coupling of VOF with LS proposed by Albadawi et al. [10] is incorporated into OpenFoam-v1706 to treat this weakness and assess its potential for liquid jet atomization.

II. NUMERICAL MODEL

A. Governing Equation

The governing equations for two isothermal, incompressible, and immiscible fluids, including the mass and momentum conservation are given by the followings, respectively [11]:

$$\nabla.V = 0 \tag{1}$$

$$\frac{\partial(\rho V)}{\partial t} + \nabla.(\rho V V) = \nabla.T - \nabla p_d - g.x\nabla\rho + F_\sigma \tag{2}$$

Where V is the velocity vector field, p_d is the pressure , ρ is the fluid density, μ is the fluid viscosity, T is the viscous deformation tensor given by $T = \nabla.(\mu\nabla U) - \nabla U\,.\nabla\mu$, x is the position vector, g is gravitational acceleration, and F_σ is the volumetric surface tension force.

B. Volume of Fluid

The Volume of Fluid advection equation based on the OpenFoam formulation [11] is given by:

$$\frac{\partial F}{\partial t} + \nabla.(V\,F) + \nabla.[V_r F(1-F)] = 0 \tag{3}$$

F is the volume fraction equal to unity in the liquid phase, zero in the gas phase, and value between 0 and 1 in interfacial regions. In addition, V_r is the relative velocity between the two phases. The relative velocity V_r plays the role of compressive flux in this formulation and thus must be limited to the maximum velocity field in the whole computational domain as follows [9]:

$$|V_r| = min[c_\alpha|V|, max(|V|)] \tag{4}$$

Where c_α is a compression coefficient with a value greater than 1 [10] . In our study, c_α is chosen to be 1.5.

Fluid properties such as viscosity μ and density ρ at any point in the domain are calculated as the weighted average of the volume fraction of the two fluids as the following [11]:

$$\mu = \mu_l F + \mu_g(1-F) \tag{5}$$

$$\rho = \rho_l F + \rho_g(1-F) \tag{6}$$

Where μ_l and μ_g are the viscosity of the liquid and the gas, respectively, while ρ_l and ρ_g are the density of liquid and gas, respectively [11].

The local curvature k is calculated by taking the divergence of the unit normal vector of the phase interface $\hat{n}$ as follows [2]:

$$k = -\nabla.\hat{n} = -\nabla.\left(\frac{\nabla F}{|\nabla F|}\right) \tag{7}$$

The surface tension force F_σ is calculated based on the continuum force model introduced by Brackbill et al. [12] as follows:

$$F_\sigma = \sigma k \nabla F \tag{8}$$

Where σ is the surface tension coefficient.

C. Simple Coupled Level Set and Volume of Fluid (SCLSVOF)

Albadawi et al. [10] proposed a simple method of coupling the Volume of Fluid with the level set, namely SCLSVOF. In the SCLSVOF method, a new scalar field, namely level set ϕ, which represents the shortest sign distance to the interface, is added. Even though two fields define the interface, namely F and ϕ, only F in equation (3) is advected. Albadawi et al [10] suggested that the initial value of ϕ_0 is given by:

$$\phi_0 = (2F-1).\xi \tag{9}$$

Where ξ is a dimensionless parameter related to the mesh size $\triangle x$. It is suggested that ξ should be set to $0.75\triangle x$ [10]. The value of ϕ_0 is re-distanced using the approach proposed by Sussman et al. [8] as follows:

$$\frac{\partial\phi}{\partial\tau} = sign(\phi_0)(1-|\nabla\phi|) \tag{10}$$

The initial condition is as follows [2]:

$$\phi(x,0) = \phi_0(x) \tag{11}$$

Where, τ is a fictitious time, and $sign$ is the sign function. The number of iterations (ϕ_{corr}) of equation (10) is limited [10], and has to satisfy the condition:

$$\phi_{corr} = \frac{\epsilon}{\triangle\tau} \tag{12}$$

Where ϵ represents the thickness of the interface, which defines the transition region between the two phases. In this study, ϵ is equal to $1.5\triangle x$. Once we define the smoothed

level set, we re-compute the unit normal of the interface $\hat{n}$ as a function of the level set as follows [2]:

$$\hat{n} = \frac{\nabla\phi}{|\nabla\phi)|} \tag{13}$$

The local curvature is also re-computed using the continuous function ϕ by taking the divergence of equation (13) as $k = -\nabla.\hat{n}$. Moreover, the volumetric surface tension force in equation (8) is re-computed as follows [8]:

$$F_\sigma(\phi) = \sigma k(\phi)\delta_\epsilon(\phi)\nabla\phi. \tag{14}$$

Where δ_ϵ is the smoothed Dirac function used to smooth the surface tension effect to a limited region near the interface and defined as [10]:

$$\delta_\epsilon(\phi) = \begin{cases} \frac{1}{2}[1 + cos(\frac{\pi\phi}{\epsilon})] & if\ |\phi| \leq \epsilon \\ 0 & otherwise \end{cases} \tag{15}$$

The physical properties are smeared over a fixed thickness of the interface using the smoothed Heaviside function H_ϵ defined as [10]:

$$H_\epsilon(\phi) = \begin{cases} 1 & If\ \phi > \epsilon \\ \frac{1}{2}[1 + \frac{\phi}{\epsilon} + \frac{1}{\pi}sin(\frac{\pi\phi}{\epsilon})] & If\ |\phi| \leq \epsilon \\ 0 & If\ \phi < \epsilon \end{cases} \tag{16}$$

Thus, the physical properties, namely the density and the viscosity, are calculated as follows [10]:

$$\rho(\phi) = \rho_g + (\rho_l - \rho_g)H_\epsilon(\phi) \tag{17}$$

$$\mu(\phi) = \mu_g + (\mu_l - \mu_g)H_\epsilon(\phi) \tag{18}$$

Accordingly, the momentum equation can be re-written as a function of the level set as follows [8]:

$$\frac{\partial(\rho V)}{\partial t} + \nabla.(\rho VV) = \nabla.T - \nabla p_d - g.x\nabla\rho(\phi) + F_\sigma(\phi) \tag{19}$$

Details of the finite volume discretization of the continuity, momentum, and volume fraction advection equations in interFoam can be found in [11].

III. NUMERICAL VALIDATION OF SCLSVOF METHOD

A. A 2D droplet in vortical field

The advection algorithm for stretching and thinning of a 2D droplet in a vortical flow field was tested. This test introduced by Rider et al. [13] aims to evaluate the capability of the solver to handle severe deformation without causing a fictitious numerical breakup. The test case consists of 2D droplet of radius 0.15 located at (0.5, 0.75) in 1×1 square domain. The velocity field is given by a time-dependent stream function $\Psi(x, y, t)$ as follows [13]:

$$\Psi(x, y, t) = \frac{1}{\pi}\sin^2(\pi x)\sin^2(\pi y)\cos(\frac{\pi t}{T}) \tag{20}$$

Where T is the flow period suggested to be 8 [9]. The velocity field deforms the droplet into a thin spiraling ligament where the maximum deformation occurs at $t = T/2$. Then, the velocity field reverses the flow, restoring the initial shape at t = T. The advection error ε_{RK2D} based on [13] is defined as:

$$\varepsilon_{RK2D} = \sum_{j=1}^{N} A_j|F_j^I - F_j^F| \tag{21}$$

Where N is the total number of the computational cells, A_j is the area of the indexed computational cell, F_J^I and F_J^F are the initial and final volume fractions, respectively. Three levels of grid resolutions, namely 32×32, 64×64, and 128×128 are used in the test. The performance of the SCLSVOF solver is compared with the following methods: the geometrical advection approach, namely (PLIC) introduced by Rider et al. [13], the hybrid level set method introduced by Aulisa et al. [14], and algebraic advection algorithm (THINC-SW) introduced by Xiao et al. [15], which uses hyperbolic tangent representation for the volume fraction field.

Fig 1 shows the initial, starching the final shape of Rider test of 2D droplet with 128×128 grid resolutions. Errors of the advection algorithmsε_{RK2D} are shown in Table I.

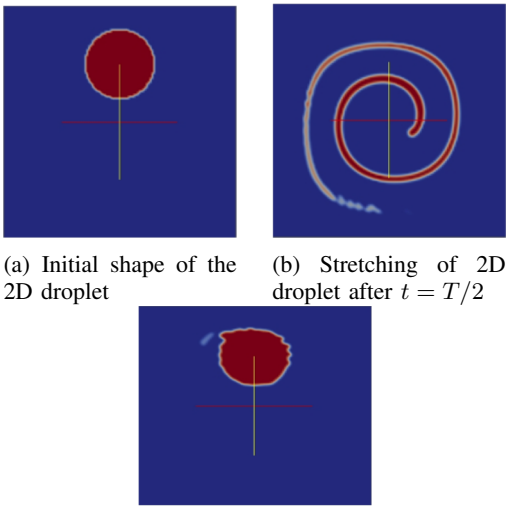

(a) Initial shape of the 2D droplet

(b) Stretching of 2D droplet after $t = T/2$

(c) Final shape of droplet after $t = T$

Fig. 1: Figs. 1a, 1b, 1c show the initial, starching the final shape Rider test of 2D droplet with 128×128 grid resolutions

From Table I, it can be noticed that the error ε_{RK2D} resulting from SCLSVOF is in the same order of magnitude as the error ε_{RK2D} resulting from PLIC [13] and THINC-SW [15] with a value that is slightly higher, and is one order of magnitude less than hypird level set [14].

The algorithm introduced by Aulisa et al. [14] shows superiority in this type of flows (vortical flow) compared to the algorithms shown in Table I.

TABLE I: THE COMPARISON OF ε_{RK2D} ERRORS RESULTING FROM SCLSVOF WITH THE THREE METHODS [13], [14], and [15] FOR THE THREE GRID RESOLUTIONS

Method	Grid Resolution		
	32×32	64×64	128×128
PLIC [13]	0.0478	0.00698	0.00144
Hypird Level Set [14]	0.0253	0.00278	0.00048
THINC-SW [15]	0.039	0.0152	0.00396
SCLSVOF	0.085115	0.0223	0.00626552

B. 2D Standing Capillary Wave

A sinusoidal wave is perturbed and allowed to evolve under the influence of surface tension force. The test aims to investigate the solver performance in a high Ohnesorge number where the viscosity effect overcomes the surface tension. The setup of the simulation is shown in Fig. 2. The properties of each phase are provided in the figure. The surface tension coeffient is $\sigma = 0.07N/m$. The initial amplitude and the wavelength λ are $1 \times 10^{-5}\,m$ and $1 \times 10^{-4}\,m$, respectively. The sides are of periodic boundary conditions for all fields. We used four different levels of computational cell numbers: corset with 10×50, coarse with 20×100, fine with 40×200, and finest with 80×400 in x and y directions, respectively. All grids are uniformly structured. The surface elevation γ_{decay} and wave frequency ω_{anal} can be analytically calculated as follows [16]:

$$\gamma_{decay} = 2\nu K^2 \tag{22}$$

$$\omega_{anal} = \sqrt{\frac{\sigma K^3}{\rho_1 + \rho_2}} \tag{23}$$

Where ν is the kinmetic viscosity, K is the wave number given by $2\pi/\lambda$, ρ_1 and ρ_2 are densities of the two phases, respectively. The decay rate of the free surface is calculated as $\exp(-\gamma_{decay} t)$ [16].

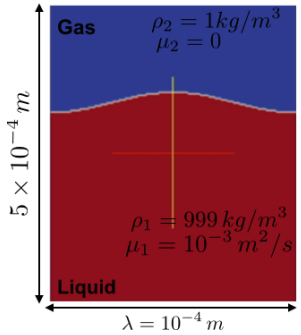

Fig. 2: Standing capillary wave setup

Figs. 3 and 4 show the decay of the surface elevation obtained by inteFoam and SCLSVOF methods for the four grid resolutions, respectively. A Matlab script is used to find the position of the surface at a value of F = 0.5.

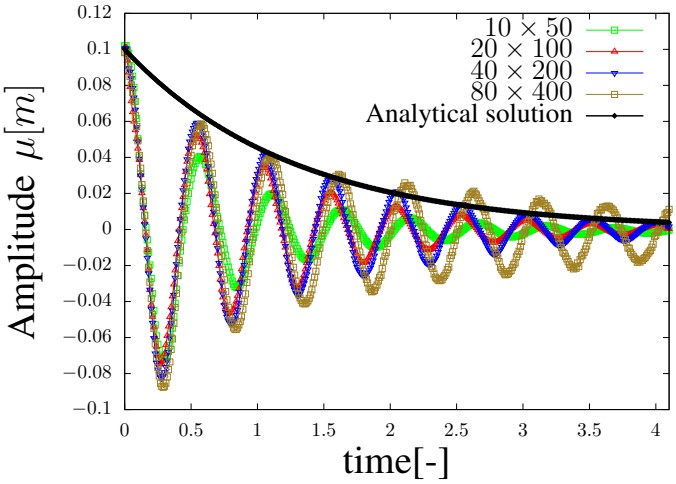

Fig. 3: The decay rate of the surface elevation obtained by interFoam for the four grid resolutions

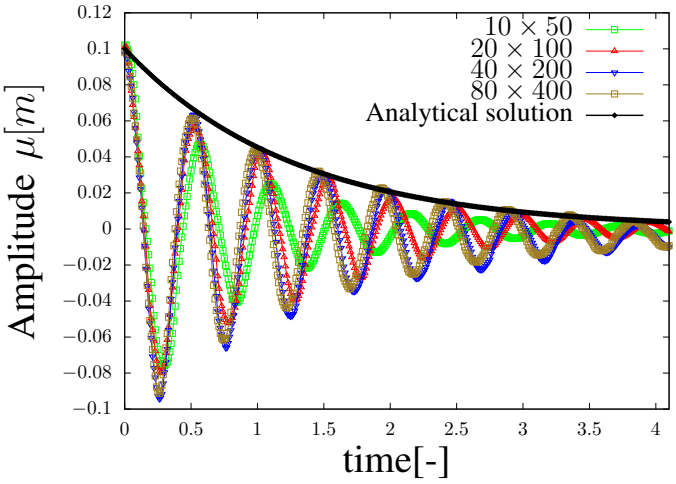

Fig. 4: The decay rate of the surface elevation obtained by SCLSVOF for the four grid resolutions

The results obtained by the interFoam method for the surface elevation position do not fit well with the analytical solution. The computed surface elevation overshoots as the grid resolution increases to the finest. On the other hand, the computational results obtained from the SCLSVOF method, as shown in Fig. 4, show better agreement with the analytical solution. The finest grid resolution is sufficient to evaluate the performance of the SCLSVOF method on the decay rate.

Table II shows the relative percentage error of the wave frequency resulting from interFoam and SCLSVOF for the four grid resolutions.

Table II indicates that the error in the wave frequency obtained by the interFoam method decreases as the mesh resolution increases. However, a shift of the wave frequency is noticeable in the case of the finest grid resolution as time goes by yielding increases in the frequency error by 29% compared to the error obtained for the fine grid case. This type of instability was also

TABLE II: RELATIVE ERROR (%) OF THE CAPILLARY WAVE FREQUENCY OBTAINED BY INTERFOAM AND SCLSVOF METHODS

Numerical methods	Coarsest	Coarse	Fine	Finest
interFoam	13.3041	5.88936	4.435	5.6432
SCLSVOF	14.0346	5.466	4.3458	2.843

observed by [3] and denoted as the nonlinearity effect. On the other hand, the frequency error obtained by the SCLSVOF method decreases as the grid resolution increases, and no shift in wave frequency occurs.

C. Static drop in equilibrium with different varying density ratios

The pressure jump across a static drop in a zero net gravity field was computed. The exact pressure jump value $\triangle P_{Exact}$ across the interface is given by the Laplace-Younge equation as follows [9]:

$$\triangle P_{Exact} = \sigma k \tag{24}$$

This test introduced by Francois et al. [17] aims to examine the solver's ability to handle desecrate force balance between the pressure jump and the surface tension for different density ratios. The error in the pressure jump is directly associated with the local curvature computation. The test case consists of a static drop positioned at the center of a square computational domain of 8×8 m. The radius of the drop is $R = 2\,m$. The number of computational cells used in the simulation is 40×40 in the x and y direction, respectively. The kinematic viscosity for both phases is zero. Three different density ratios are used in the simulations, namely 10^2, 10^3, and 10^5. The surface tension coefficient is $\sigma = 73 N/m$. The exact curvature of the drop is calculated as $k = \frac{1}{R}$ [17]. Thus, the exact pressure jump is $\triangle P_{Exact} = 36.5$. In all tests, no-slip and zero gradient boundary conditions were applied to the velocity and pressure fields, respectively. The results were obtained after one time step of $10^{-6} s$. Fig .5 shows the initial setup of the test case.

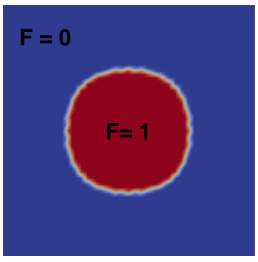

Fig. 5: Static liquid droplet in zero net gravity field

Figs. 6 and 7 show the computed pressure along x direction for the three density ratios of the drop test case with interFoam and SCLSVOF methods.

The pressure jump computed by both methods doesn't converge to the exact solution of 36.5, independent of the density ratio. However, the SCLSVOF method enhances the accuracy

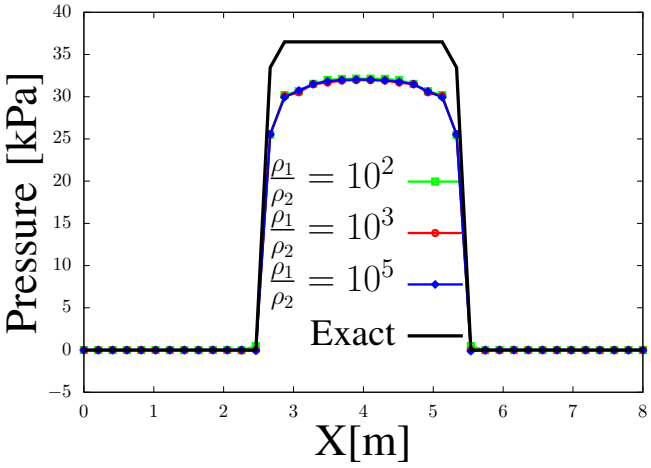

Fig. 6: Pressure variation field along x-direction for the static drop with three different density ratios using InterFoam method

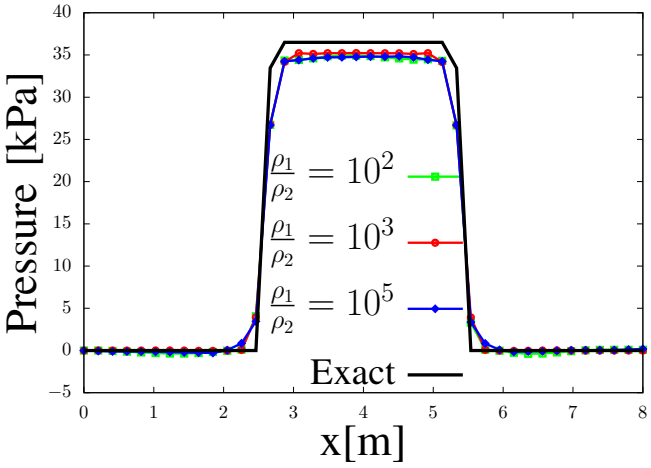

Fig. 7: Pressure variation field along x-direction for the static drop with three different density ratios using SCLSVOF method

of the computed pressure compared to interFoam results, as observed from Fig. 7 compared to Fig .6.
The error in the computed pressure is nearly 12.3248% in the case of using interFoam, and almost 4% when using SCLSVOF. Thus, a reduction by approximately 8.3287% in the error of the computed pressure value was achieved.

IV. 3D SIMULATION OF LIQUID JET IN QUIESCENT GAS

3D simulation of a fuel jet in highly pressurized gas was conducted. The simulation condition is similar to that conducted by [4], where fuel with a velocity of 50 m/s is injected from a round nozzle with a diameter of 0.1 mm into quiescent gas. The details of the fuel and gas properties are shown in Table III. The ambient pressure and the surface tension coefficient are 3 MPa and $\sigma = 0.03$ N/m, respectively.

These conditions are subjected to Reynolds, Weber, and Mach numbers of 740, 3750, and 0.14, respectively. Conducting DNS or grid dependency tests for such flow conditions requires an extremely huge amount of computational resources [4]. Moreover, experimental data for the full-time sequence of the primary breakup of such cases is unavailable. Therefore, the validity of SCLSVOF will consider its capability to physically elucidate the atomization process in terms of capturing smooth droplets, ligaments, and the other phenomena observed by Shinjo et al. [4] where more than 400 million cells were used, yet not considered DNS [4].

TABLE III: LIQUID AND GAS PROPERTIES

Liquid density (Kg/m^3)	Gas density (Kg/m^3)	Liquid viscosity $\mu_l(pas)$	Gas viscosity $\mu_g(pas)$
848	34.5	2870×10^{-6}	19.7×10^{-6}

The simulation was carried out on Galileo supercomputer (Located at CINECA in Bologna, Italy) using 80 million computational cells.

A. *Results and Discussions*

Fig. 8 shows the liquid jet emanated from the nozzle after 12 μs.

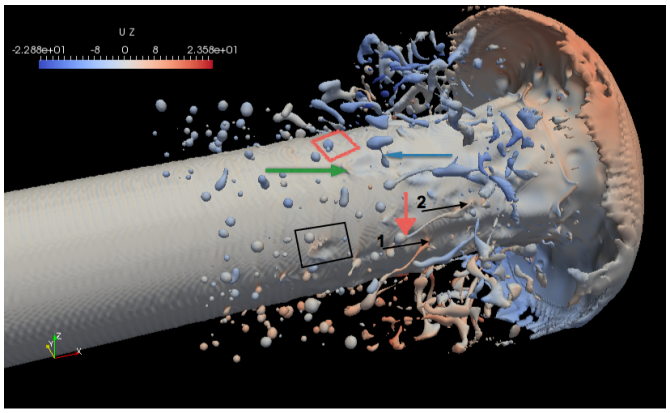

Fig. 8: Evolution of the liquid jet after 12μs using SCLSVOF methods

The jet tip exhibits an umbrella-like shape, as expected. Ligaments and droplets of different sizes with smooth surfaces are well captured. It can be noticed that two long wavy ligaments generated from the liquid core are shown by the two black arrows 1 and 2, respectively. The red arrow shows a blob at the end of ligament number 2. The green arrow shows the crest on the liquid surface explored by [4]. Another crest with droplets close to it is shown in the black square. Many crests are captured in Fig. 8, but our focus will be dedicated to the evolution of the crests indicated by the black box and the green arrow. Attention will also be paid to the droplet indicated by the red square and the liquid bulk indicated by the blue arrow.
Figs. 9 and 10 show the evolution of liquid jet emanated from the nozzle after 12.5 μs and 13 μs, respectively.
It can be seen that the ligament indicated by the black arrow number 1 shown in Fig. 8 has detached from the liquid core due to the surface tension effect as demonstrated in Fig.9.
The blob denoted by the red line shown in Fig. 8 has been pinched off by the effect of surface tension, as we can see in Fig. 10. The droplets close to the crest indicated by the black box shown in Fig. 8 has collided with it as shown in Fig. 9, then the crest starts to generate more droplets as shown in Fig. 10. It can be observed that the droplet indicated by the red square in Fig. 8 has collided with the jet surface, as shown in Fig. 9 and then has become crest as shown in Fig. 10. The liquid bulk indicated by the blue arrow shown in Fig. 8 has detached from the big bulk because of the surface tension effect, as shown in Fig. 9 to collied with crest denoted by the green arrow as shown in Fig. 10. As a result, the action of droplets re-collision with jet surface and creation of crests appear to be one the primary source of droplet formation that need more investigations.
Figs. 11 and 12 show the evolution of the the fuel jet emanated from the nozzle after 20μs and 24 μs, respectively.
It can be noticed that the region behind the jet tip is highly

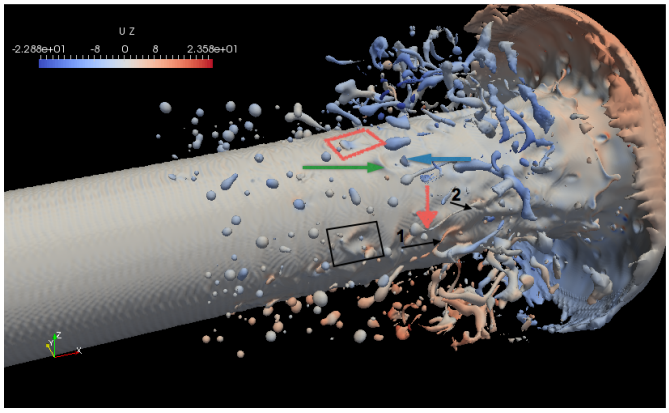

Fig. 9: Evolution of the liquid jet after 12.5μs using SCLSVOF methods

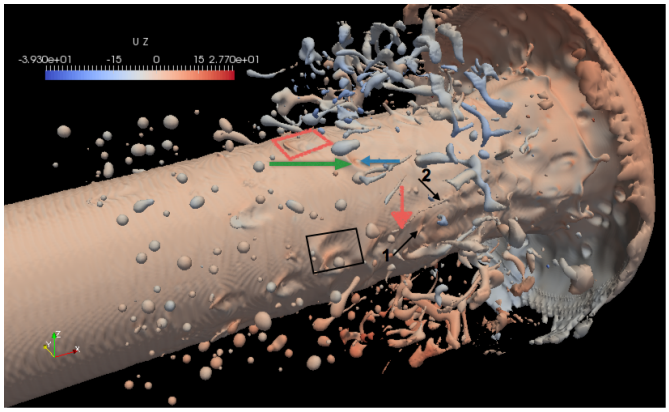

Fig. 10: Evolution of the liquid jet after 13μs using SCLSVOF methods

Fig. 11: Evolution of the liquid jet after 20μs using SCLSVOF methods

Fig. 12: Evolution of the liquid jet after 24μs using SCLSVOF methods

disturbed which conveys disturbances and waves upstream as shown in Figs. 11 and 12. As a result, droplets and ligaments are also generated from the jet surface. More computational resources are needed for detailed quantitive analysis of the atomization process. Future work will be dedicated to this issue.

Conclusion

In this present work, a numerical method, namely SCLSVOF, has been incorporated into the source code of OpenFoam software. The solver performance was validated on different varieties of tests such as droplet deformation in a vortical flow field, capillary wave with a high Ohnesorge number, and static drop in equilibrium. It is concluded that the new solver can handle severe shear deformation with an error of the same order of magnitude as other algebraic and geometrical advection approaches. The capillary wave test proves that the SCLSVOF method performance is more efficient than interFoam in high viscous incompressible multiphase flow. Moreover, the static drop test proves the efficiency of the new algorithm in enhancing the accuracy of the computed pressure across the interface compared to the interFoam solver. Thus, The preliminary results indicate that the SCLSVOF method appears more robust in surface tension-dominated flow than interFoam method. Finally, the new solver's ability to physically elucidate the atomization of a turbulent liquid jet in a quiescent gas was assessed. The new solver managed to catch the flow motion of the jet. Moreover, droplets and ligament formation were well captured. As a result, the new method tends to have good potential in simulating and modeling the atomization of a turbulent liquid jet.

References

[1] M. Herrmann, "Detailed numerical simulations of the primary atomization of a turbulent liquid jet in crossflow," *Journal of Engineering for Gas Turbines and Power*, vol. 132, no. 6, 2010.

[2] T. Ménard, S. Tanguy, and A. Berlemont, "Coupling level set/vof/ghost fluid methods: Validation and application to 3d simulation of the primary break-up of a liquid jet," *International Journal of Multiphase Flow*, vol. 33, no. 5, pp. 510–524, 2007.

[3] O. Desjardins, V. Moureau, and H. Pitsch, "An accurate conservative level set/ghost fluid method for simulating turbulent atomization," *Journal of computational physics*, vol. 227, no. 18, pp. 8395–8416, 2008.

[4] J. Shinjo and A. Umemura, "Simulation of liquid jet primary breakup: Dynamics of ligament and droplet formation," *International Journal of Multiphase Flow*, vol. 36, no. 7, pp. 513–532, 2010.

[5] C. W. Hirt and B. D. Nichols, "Volume of fluid (vof) method for the dynamics of free boundaries," *Journal of computational physics*, vol. 39, no. 1, pp. 201–225, 1981.

[6] A. Baraldi, M. Dodd, and A. Ferrante, "A mass-conserving volume-of-fluid method: volume tracking and droplet surface-tension in incompressible isotropic turbulence," *Computers & Fluids*, vol. 96, pp. 322–337, 2014.

[7] A. Dervieux and F. Thomasset, "A finite element method for the simulation of a rayleigh-taylor instability," in *Approximation methods for Navier-Stokes problems*, pp. 145–158, Springer, 1980.

[8] M. Sussman, P. Smereka, and S. Osher, "A level set approach for computing solutions to incompressible two-phase flow," *Journal of Computational physics*, vol. 114, no. 1, pp. 146–159, 1994.

[9] S. S. Deshpande, L. Anumolu, and M. F. Trujillo, "Evaluating the performance of the two-phase flow solver interfoam," *Computational science & discovery*, vol. 5, no. 1, p. 014016, 2012.

[10] A. Albadawi, *On the assessment of numerical interface capturing methods for two fluid flow applications*. PhD thesis, Dublin City University, 2014.

[11] M. Damian, "S. description and utilization of interfoam multiphase solver," 2012.

[12] J. U. Brackbill, D. B. Kothe, and C. Zemach, "A continuum method for modeling surface tension," *Journal of computational physics*, vol. 100, no. 2, pp. 335–354, 1992.

[13] W. J. Rider and D. B. Kothe, "Reconstructing volume tracking," *Journal of computational physics*, vol. 141, no. 2, pp. 112–152, 1998.

[14] E. Aulisa, S. Manservisi, and R. Scardovelli, "A mixed markers and volume-of-fluid method for the reconstruction and advection of interfaces in two-phase and free-boundary flows," *Journal of Computational Physics*, vol. 188, no. 2, pp. 611–639, 2003.

[15] F. Xiao, S. Ii, and C. Chen, "Revisit to the thinc scheme: a simple algebraic vof algorithm," *Journal of Computational Physics*, vol. 230, no. 19, pp. 7086–7092, 2011.

[16] H. Lamb, *Hydrodynamics*. Cambridge university press, 1932.

[17] M. M. Francois, S. J. Cummins, E. D. Dendy, D. B. Kothe, J. M. Sicilian, and M. W. Williams, "A balanced-force algorithm for continuous and sharp interfacial surface tension models within a volume tracking framework," *Journal of Computational Physics*, vol. 213, no. 1, pp. 141–173, 2006.